International Journal of Thermal Sciences 118 (2017) 53–68

Contents lists available at ScienceDirect

International Journal of Thermal Sciences

journal homepage: www.elsevier.com/locate/ijts

Steady state experimental investigation of thermal contact conductance between curvilinear contacts using liquid crystal thermography

Surya Kumar, Andallib Tariq*

Department of Mechanical and Industrial Engineering, Indian Institute of Technology Roorkee, Roorkee, 247667, India

ARTICLE INFO

Article history:
Received 22 August 2016
Received in revised form
14 April 2017
Accepted 15 April 2017

Keywords:
Thermal contact conductance
Thermal contact resistance
Interface
Curvilinear contact
Liquid crystal thermography

ABSTRACT

Heat transfer components comprise of several types of metallic contacts. Commencing from the conventional conforming rough surface contact combinations, the situation might culminate in terms of the complex non-conforming rough curvilinear contacts of the real heat transfer devices. Available theoretical models fail to correctly predict thermal contact conductance (TCC) over the broader range of influencing parameters, even for the simplest geometry, and thus experiments plays a pivotal role in the field. Researchers are indefatigably working for developing accurate experimental methodologies to get precise estimate of TCC, and create broader database of results for upcoming theoretical models.

In this regard, this paper presents steady state thermal contact conductance analysis on two solid bodies of brass, carrying flat and curvilinear contact combinations, under variable loading conditions ranging in between 0.27 and 4.0 kN. A customized and standardized experimental set up has been used to measure steady state TCC for three different types of geometrical configurations, which are flat-flat, cylinder-flat and cylinder-cylinder contacts. At the start, TCC has been evaluated on the basis of centrally placed high response, super accurate, ungrounded thermocouples, which are mounted axially across the contacting bodies. In the later part of the paper, an optical, non-invasive and inexpensive method, based upon liquid crystal thermography (LCT) has been implemented to get the precise estimate of TCC for different configurations under consideration. The region close to the interface, which has the profound effect on the axial temperature distributions, is identified. Eventually, the separation region, where dramatic variation in the thermal conductivity occurs and classical Fourier law tends to fail has been identified. The separation region is further segregated in sub-regions on the basis of distinct temperature zones, which allows estimating the effective thermal conductivity of the materials in gap. The precise temperature jump close to the interface is extrapolated, and consequentially used to predict the steady state TCC for all three geometrical configurations. The value of TCC is evaluated again on the basis of effective thermal conductivity concept, and the results have been compared together. The present investigation establish a unique methodology for TCC estimation on the basis of steady state liquid crystal (LC) measurements, and provide valuable insight of heat transfer across the curvilinear contacts, and can be treated as the base line measurements for any of the upcoming scale resolved numerical models.

1. Introduction

Accurate knowledge of heat transfer occurring through interfaces of metallic bodies in contact is of great concern in the designing of microelectronics cooling, nuclear reactor cooling, heat exchangers and thermal control systems for spacecraft applications. Furthermore, many of the times, the interface resistances might be small, however they becomes critical in structures where there are numerous interfaces, such as super-lattices and ultra large scale integrated circuits. Evidently, the heat transfer across the interface is influenced by a number of parameters, including the thermophysical and mechanical properties, surface roughness and contact loading. When two solid surfaces form a contact, presence of surface roughness limits their physical contacts to a limited

* Corresponding author.
E-mail address: tariqfme@iitr.ac.in (A. Tariq).

http://dx.doi.org/10.1016/j.ijthermalsci.2017.04.014
1290-0729/

number of discrete points at their interface. This imperfection causes a constriction in the heat transfer at the interface termed as thermal contact resistance and its reciprocal is called thermal contact conductance (TCC) and is defined as:

$$h = \frac{Q/A_c}{\Delta T} = \frac{q}{\Delta T} \quad (1)$$

where Q is the heat transfer through the interface of two contacting solid, A_c is the contact area, ΔT is the temperature jump at the interface, and q is the average interfacial heat flux.

A large number of theoretical and experimental investigations on interfacial heat transfer have been carried out over the last five decades as compiled by Yovanovich [1] and Fletcher [2]. Cooper et al. [3] developed surface deformation model as well as thermal model to predict thermal contact resistance which became a benchmark for many models developed subsequently. Later, Mikic [4] proposed theoretical formulations of TCC on the basis of modes of deformation of contact surfaces for nominally flat surfaces. Jeng et al. [5] developed a TCC model by considering elastic, plastic and elastoplastic deformation of the asperities and compared the predicted results with the experimental data. Most of the theories tend to overpredict or underpredict the estimated TCC derived from the experimental measurements as models and correlations developed are suitable for only limited conditions. Recent work [6] highlighted the limitation of available models in which the fraction of proposed real contact area is relatively small and the contact spots are assumed to be circular and separated. It was also argued that these aforesaid two assumptions were not valid in the conditions characterized by large fractions of real contact area. These limitations of models make the experimental investigation, still an effective way to estimate the TCC for practical applications.

Based upon the detailed literature review, it has been observed that most of the experiments were performed to quantify TCC for typical flat-flat contacts. Sridhar and Yovanovich [7] performed experiments on tool steel specimens for flat-flat contacts and proposed elastoplastic model for estimating TCC. Yuncu [8] did extensive experiments on 26 pairs of steel, copper, brass and aluminum specimens and proposed that dimensionless TCC across the contacting solid spots depend on dimensionless contact pressure. Misra and Nagaraju [9] did an experimental study on flat-flat contacts to show the presence of thermal stress in contacts and its effect on TCC. Tariq and Asif [10] performed steady state experiment to calculate solid spot conductance for several experimental parameters and compared the results with the existing theoretical models. It was observed that most of the available theoretical models had limitation in correctly predicting TCC within the range of experimental parameters. Later, based upon the non-dimensional parameters, suitable generalized correlations of TCC for nominally flat metallic contacts were presented by Asif and Tariq [11] in order to fulfill the obligations for the design engineers/researchers.

Veering away from the flat-flat metallic contact, very limited amount of investigations were performed on contact conductance for cylindrical and cylinder-flat contacts due to their complex geometrical arrangements. Evidently, the value of TCC across cylindrical and cylinder-flat contacts is an important consideration for the design of a thermal system in an industry. Ayers [12] reported diverse applications of cylindrical contacts such as composite cylindrical tanks, space structures, power transmission lines, electronic devices, nuclear fuel elements, air conditioning systems, and pipelines. Madhusudana [13] presented an analysis for the prediction of the thermal conductance of cylindrical joints for radial heat flow. The value of TCC depends on the geometrical, thermos-physical and surface properties of the cylinders as well as heat flux and maximum operating temperatures. The developed theoretical model was compared with the experimental data of other researchers with minimal information on surface parameters and maximum temperature rise. Kumar et al. [14] developed a mathematical model to predict TCC between curvilinear surfaces and conducted experiments in vacuum for the measurement of TCC between stainless steel and aluminum cylindrical contacts over a range of contact pressure. It was found that the value of TCC was of lower magnitude in cylindrical contacts as compared to flat contacts. Mcgee et al. [15] presented a line contact model for the thermal resistance of a cylinder-flat contact, and compared the results with the experimental measurements. It was observed that the validity of line-contact model was dependent on limiting minimal contact loading, and below a certain value of load parameter large errors were reported along the contacting surfaces. Evidently, due to the lack of reliable theoretical models for cylinder-flat and cylindrical contacts, it is difficult to predict a definite value of TCC for any practical application. Complexity of the field calls for the dismal need towards reliable experimental investigations to predict the TCC for different curvilinear contacts, which can also act as the reliable database towards validating any of existing and upcoming theoretical modelling for estimating TCC [10].

As far as the methodologies for estimating the TCC are concerned, there exist two way to predict the TCC, namely steady state method and transient method. Zhang et al. [16] discussed about the relative merits and demerits of transient and steady state methodologies stating that, the transient experiments are of short duration compared to long duration steady state experiments. However, due to the greater precision and reliability, the steady state methodologies have been emphasized as standard procedure to determine the TCC as compared to the transient approach. Among all these experiments, thermocouples are the most conventional and widely used intrusive measurement of temperatures inside a heat conducting body. In TCC experiments, obtaining accurate interface temperature is quite essential for the correct assessment of interfacial temperature jump. In the conventional approach, temperature jump across the interface is estimated by extrapolating temperature gradient measured far from the interface. Significant work on extrapolation error was published by Thomas [17]. As much as 19% extrapolation error was reported in the calculation of interfacial temperature jump. This extrapolation error will substantially affect the correct realization of TCC. Several researchers have explained the demerits and limitation of intrusive way of temperature measurements. Woolley and Woodbury [18] reported that the use of thermocouples inside a heat conducting body distorts the temperature field in the body and which may lead to a significant bias in the temperature measurement. Fieberg and Kneer [19] noted that temperature measurements with thermocouples modifies the thermal behavior of the bodies and tend to give inaccurate TCC results. Evidently, TCC estimate is strongly influenced by the uncertainty in elemental temperature measurement, and the degree of correct estimate of temperature jump at the interface, and therefore dismal need exist to look forward with available non-invasive tools in the field of TCC estimation.

Furthermore, the accuracy of interfacial temperature gradient is one of the major parameter which directly influences the TCC estimation while using the steady state approach. The sharp temperature drop at the interface is the outcome of the remarkably low value of real contact area (<2%) between the mating surfaces due to restricted asperities contact spots [20], which are generally of the order of few microns in height even for the smoothest surfaces. Lot of effort has been made in past, and researchers are still struggling to develop the multi-asperity theories to correctly predict the real contact area, hence in general the existing theories are believed to give correct results only for very small loads and limited contact

areas. Although, several studies have been performed to reconstruct the surfaces with remarkable resemblance to actual surface topographies while using both deterministic and fractal models. However, their application is limited by the degree of rigor of the procedure implemented to gather the roughness data in terms of actual fine-scale topography measurements (either on the basis of analog data using profilometry, or as digital maps using microscopy), followed by processing of the measured data to fit the respective mathematical models. Recently [21], rather than making any assumptions pertaining to the shape, size, and height of the asperities and ensuing contacts, the topography of the interface is stochastically reconstructed from commonly measured surface roughness descriptors. Eventually, a method based upon the stochastically reconstruction of the topography of the two metallic surfaces was developed to extract the effective thermal conductivity, $k_{contact}$ and the TCC. All the fine-scale features of the interface including the air pockets were resolved, and the temperature distribution result for a 2-D model of contact between surfaces was presented. Subsequently, the effective thermal conductivity, $k_{contact}$ across the interface had been derived from thermal resistance based formulation.

In this connection, the advent of modern optical tools along with emerging computational capabilities can offer a solution to implement the actual reconstruction of interface while using multiscale models, and thus help in evolving the finer understanding of thermal transport across the interface. These studies essentially requires a close-up view at the interface in terms of the accurate database of 2-dimensional temperature distribution at the interface to validate the upcoming theoretical models based upon the actual topography of the surfaces. Not only this, many of the inverse transient approaches are often used to get the estimate of TCC, however they are found to be very sensitive to the measurement errors, especially the near interface measurements. Moreover, the correct estimate of TCC based upon the steady state approach also requires the precise measurement of temperature jump just across the interface. Therefore, the correct realization of the TCC by using any of approaches, directly depends upon the accuracy in temperature drop measurement, and intimacy of the sensor location with the interface.

Additionally, determining the temperature distribution at the interface has long been a topic of great interest in the field of contact mechanics/tribology. Accurate knowledge of the temperature rise in such a scenario is critical for performing thermal stress analysis between the bodies, or thermal wear modelling both of which are relevant to many engineering applications. Furthermore, with the advent of nanostructures and nanocomposite materials, thermal transport across interfaces at much smaller length scale is becoming increasingly important, where it is seldom possible to adopt the conventional thermocouple approach. Recent era have witnessed a rapid progress in the manufacturing of microelectronic and thermoelectric devices, and with continuous decrease in the size of devices and structures, heat transfer on the micro-scale is becoming a bottleneck for the development of many technologies. Certainly, microscale heat transfer analysis is unconventional and often challenging, since the Fourier heat conduction equation or continuum assumption fails as the characteristic dimension of the structures becomes comparable to the mean free path of energy carriers in semiconductors (photons) and metals (electrons), and thus more sophisticated analysis is required. When switching from a macroscopic to a microscopic approach, a difficulty encountered is the lack of knowledge in statistical thermodynamics and mechanics that are required for the microscopic analyses, which seriously limits the development of the model [22]; because the micromechanics itself may take years to become fully acquainted with. Interestingly, in the context of the interfacial heat transfer and TCC problem, the surface roughness plays an important parameter in restricting the heat flow, which is often limited to be of the order of few microns. Therefore, *classical size effects* [23] might be important during heat transfer in the immediate vicinity of the interface. At the interface heat transfer seep through the actual contact spots, and therefore the characteristic length is reduced to be comparable to the size of roughness, hence the energy carrier propagating through the medium has numerous collisions with the boundaries, and these collisions further impede the energy from top to bottom. Although, these phenomena of heat transfer requires the deep understanding of microscale heat transfer in solids and can be better understood [23] by using a variety of theoretical approaches including the Boltzmann transport equation, molecular dynamics, the Landauer formalism, the Green-Kubo formalism, radiation analogies, and other techniques; however in the present scope of investigation, a closer perspective of temperature profile with higher spatial resolution based measurement at the interface might be useful in defining the effective thermal conductivity, and subsequently the TCC across the interface.

Recently, some nonintrusive methods such as Laser photothermal method [24,25] and infrared thermography (IR) method [19,26] have been employed to investigate TCC at the interface of two contacting bodies. Though these above nonintrusive methods have effectively dealt with problems associated with intrusive methods but are expensive to implement. From the technique perspectives, researchers [27–29] have also suggested a more economical and convenient way to measure surface temperature of a heat conducting body by implementing an optical based diagnostic tool, namely liquid crystal thermography (LCT) technique. LCT is a convenient non-intrusive technique that can provide temperature data over the whole region of test surface. In past, it has been extensively used for fluid mechanics related studies, electronic device testing, and medical thermology. LCT uses encapsulated liquid crystal (LC) materials, which changes pitch size of the helical molecular structure during temperature change, and thus it can be conveniently utilized as the temperature sensors. LC modifies the incident white light and display color whose wavelength is proportional to temperature. Its change in appearance is restricted over a specified range of temperatures called temperature band, and within the temperature band interval, the colors change from red to blue as a function of temperature. Additional information about the characteristics of liquid crystal and their use in thermometry and heat transfer may be found in Ireland and Jones [28] and Hallcrest™ [30]. Abdullah et al. [31] summarized a wide range of LCT applications in fluid mechanics/heat transfer problems, where LCT is extensively used as thermographic mapping technique to determine heat transfer coefficient. In their common microencapsulated form, LC might provide a high spatial resolution measurement up to the scale of 10–25 μm [32], and therefore its footprint can be seen in the emerging area of microchannel heat transfer studies. The author of this paper have also used the LCT extensively in the specific problem of ribbed flow studies [33–37], however through this investigation an effort has been made to implement the LCT in capturing the 2-D axial temperature distribution/pattern along the interface to deal with the problem of TCC estimation.

Evidently, the aforementioned discussion establishes the importance of: (*i*) TCC estimation for different curvilinear contacts in thermal engineering devices, and (*ii*) role of measurement techniques towards precisely capturing the temperature distribution at the interface. In regard to the curvilinear contacts, very limited experimental investigations exist towards estimating the TCC for the case of cylinder-flat and cylinder-cylinder contacts. Additionally, to the best of authors' knowledge, it has been observed that relatively negligible amount of work has been

performed towards capturing the microscale temperature pattern/distribution at the interface which is likely to be a novel information. Therefore, present study can be regarded as one of the frontier investigation in the pertinent field, which the author would like to report as the primary findings of ongoing investigations with an aim to provide the interface between the macroscopic and microscopic heat transfer at the interface with the help of high resolution optical based measurement technique.

2. Instrumentation and measurement

A customized and standardized experimental setup [10,11] has been used in the present research to measure steady state TCC for three different types of geometrical configurations, which are flat-flat, cylinder-flat and cylinder-cylinder contacts. Brass metal is chosen for all the geometrical configurations of the specimens, because of its wider applications in heat transfer equipment. Firstly, the whole test assembly is placed in vacuum environment to minimize heat loss to the environment and steady state experiments have been performed on a flat-flat contact. Temperature data have been recorded with the thermocouples mounted at different axial locations in the contacting bodies. Experimental result of flat-flat contact has been compared with the existing theoretical models to standardize the setup. Subsequently, the steady state experiments have been performed for curvilinear contacts and important parameters affecting TCC has been investigated. Later, in the second part of this work, an optical, non-intrusive, and relatively less expensive thermographic technique, i.e. LCT has been used for the very first time for mapping surface temperatures of two contacting bodies for TCC investigation. Self-adhesive prefabricated LC sheets (LCR Hallcrest™), which contains an extremely thin film of the liquid crystals, sandwiched between a transparent polyester sheet and a black absorbing background have been used for temperature mapping. The thickness of the micro-encapsulated temperature sensitive LCs are generally of the order of 10–15 μm [27–32] with an overall thickness of the sheet 100 μm. Very accurate estimate of temperature jump at the interface has been mapped with the help of LCT, whose spatial resolution is quite high and is of the order of few microns (depends upon the camera hardware and lenses combinations). LCT experiments for mapping surface temperatures of contacting bodies have been performed in the ambient environment and results were presented in detail for all of the configurations at a single nominal loading condition. The details of the apparatus and instrumentations have been described well in an earlier publication by the author, and can be referred further [10,11]; however for sake of completeness, lucid details have been briefed herewith in the foregoing paragraphs, along with the additional aspect related with the LC based temperature measurements.

The basic experimental setup consists of several components, which has been shown in Fig. 1 along with the different contact configuration under study. The major components are: vacuum chamber along with pump, ball seat arrangement, insulating pads, cartridge heater, heating block, heat flux meters, thermocouples, cooling block, load cell, flexible spring bellow, and the specimens. A rotary type vacuum pump has been attached to the chamber for creating vacuum environment inside the vacuum chamber. It eliminates the convective heat transfer loss due to residual gas in the chamber. Madhusudana [38] had observed that radiation heat loss becomes significant only at high temperatures (>450 K) investigations. Presently, the maximum temperature range is well within 350 K, henceforth the effect of radiation heat transfer between contact surfaces is suitably neglected. Hydraulic jack has been used for axial loading to the lower specimen, and incorporation of flexible spring bellow at the bottom of the setup ensures vertical displacement of shaft without disturbing the vacuum conditions. A pre-calibrated load cell is used for measuring the applied load. Heat is supplied to the upper specimen by two 150 W cartridge heaters inserted into the heating block and controlled by a PID (proportional-integral-derivative) controller, and extracted from the bottom of the lower specimen with the help of cooling block, which is cooled by re-circulating the steady flow mixture of water and ethylene glycol through a PID controlled chiller. A customized and pre-calibrated solid state thin metallic transducer (HT-50 thermal flux meters from ITI, Inc USA) have been used at the top and bottom of upper and lower specimens respectively in conjunction with the specimen in use. These pre-calibrated heat flux meters are connected with a digital display system to show the heat flow rate readings.

2.1. Specimen preparation

One set of upper and lower specimen for each geometrical configuration is prepared. Each test specimen has four fine holes of 12.5 mm in depth, 0.8 mm in diameter, at different intervals for mounting the thermocouples, which has been created with the help of advanced EDM based manufacturing processes. Schematic diagram of specimens for each type of contact is shown in Fig. 1, where diameter of all the curved surfaces is kept at 25 mm. The RMS roughness and mean arithmetic average slope of the asperities of all the test surfaces are measured by using optical profilometer (Vecco Wyko NT1100). The surface microhardness measurement is made with the help of a Semi-Automatic Vicker's Microhardness tester (MVH- S Auto). The material considered is brass with an effective surface roughness $\sigma \sim 5$ μm at the contacting end for each set of specimens. Surface properties of test specimens are given in Table 1. Material properties used in the analysis are listed in Table 2.

2.2. Experimental methodology and validation

Test specimens are cleaned with acetone and assembled to form a contact and placed inside the vacuum chamber. All the surfaces except the test interface are pasted with a highly conductive silicone grease to minimize thermal contact resistance at these joints. Holes on the specimens are mounted with fast response ungrounded K type miniature thermocouples (wire diameter = 0.1 mm, with sheath diameter of 0.5 mm carrying very low temperature drift, highly accurate, super stable type). The thermocouples are embedded inside the specimen through fine holes, and affixed with the help of conductive silicone grease to provide effective thermal contact with the test specimens. Due care has been taken while placing specimens for cylinder-flat and cylinder-cylinder contacts to avoid any of the possible offset in contact, which can be disastrous from the stability perspective as well. The environment inside the vacuum chamber is maintained well below 7.0 Pa with the help of vacuum pump. Subsequently load is applied to the lower specimen followed by the heater and chiller in run, which initiate the 1-D axial heat flow across the interface until it attains the steady state condition.

Primary set of steady state experiments has been performed with the help of the thermocouples under vacuum chamber for estimating the TCC at varying loading conditions at the interface with different contact configurations under considerations. In order to validate the experimental setup and the experimental procedure, one pair of brass specimens with flat-flat type of surface contact carrying similar roughness parameters ($\sim 5\mu m$), as that of curvilinear contact models, at the contacting interface have been tested under different loading conditions inside the vacuum chamber. Eventually, the dimensionless solid spot conductance versus the dimensionless contact pressure variation has been plotted against

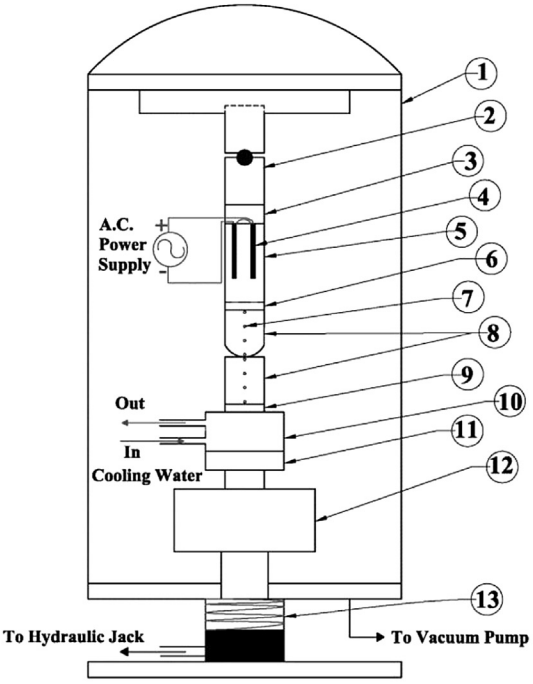

Schematic diagram of experimental setup

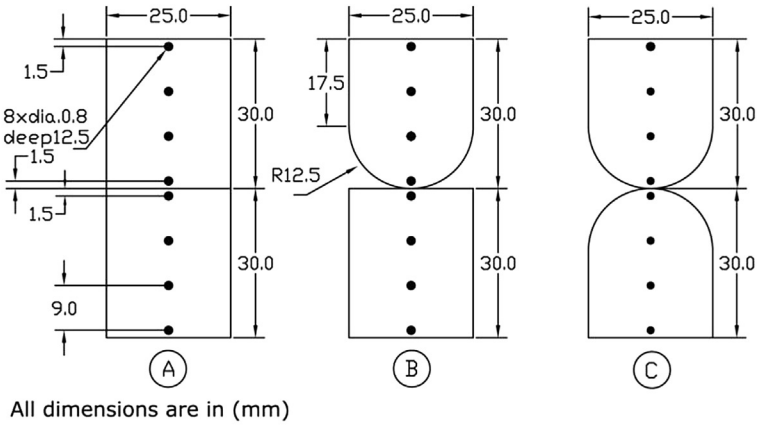

Schematic of different contact configurations

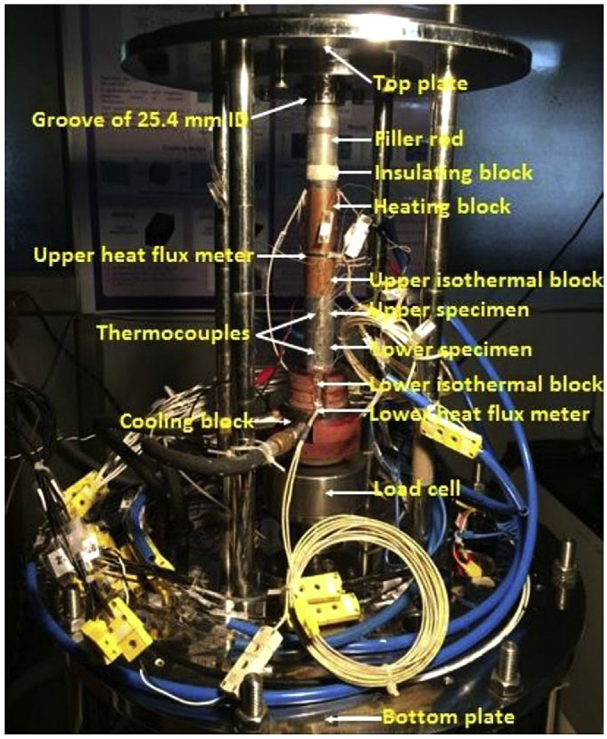

Photographic view depicting the assembly line

1 vacuum chamber
2 ball seat arrangement
3 insulating pad
4 cartridge heater
5 heating block
6 heat flux meter
7 thermocouple holes
8 upper and lower specimens
9 heat flux meter
10 cooling block
11 insulating pad
12 load cell
13 flexible spring bellow
A flat-flat contact
B cylinder-flat contact
C cylinder-cylinder contact

Fig. 1. Details of experimental facility along with schematic of specimens.

Table 1
Surface properties of specimens.

Types of configurations	Roughness parameter	
	σ	m
Flat-Flat	4.78	0.1808
Cylinder-Flat	4.55	0.2104
Cylinder-cylinder	4.76	0.2290

Table 2
Material properties of specimens.

Property	Value
k	116.0 [39]
H_v	1619.48

the established flat-flat results in Fig. 2. It has been observed that the experimental data are in good agreement with the correlation developed by Asif and Tariq [11]. Moreover, the nature of present experimental data follows the similar trend with that of the CMY [3] and Mikic [4] correlations with a fixed offset. This all confirms the validity of the present experimental set-up and the experimental procedure adopted for estimating the TCC by using the steady state measurements. In the present investigation, test system is considered to be under steady state condition, whenever the change of temperatures does not exceed by 0.1 °C in 10 min. Data

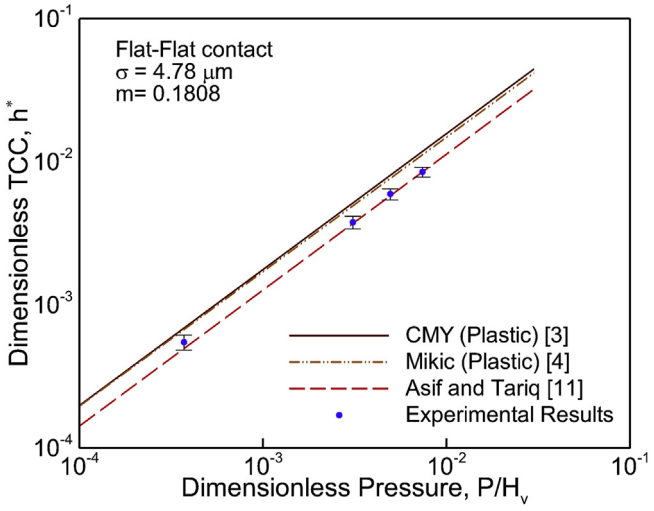

Fig. 2. Comparison between present experimental data and published correlations.

acquisition is initiated only, once the system attains the steady state condition. Finally, a comprehensive set of steady state experiments have been performed under varying loading conditions (0.274, 1.471, 2.452, 3.924 kN) with different curvilinear contact configurations under consideration.

2.3. LCT measurement and instrumentation

The experimental procedure used for estimating the TCC with thermocouples has been repeated again with the LC sheet pasted on the surface across the interface under ambient pressure condition. The thermal conductivity of the specimen (presently brass) is 116 W/m/K, whereas it is around 0.15–0.2 W/m/K for a typical LC sheet [30], and as a result, the path of least thermal resistance would involve significant conduction (600–800 times) along the metallic specimen into the region of high heat transfer. Therefore, LC sheet will truly represent the temperature of the substrate with least temperature gradient across the thickness of the LC sheet, and overall the lateral conduction through the LC sheet is supposed to be negligible. In this manner, the precise temperature mapping across the interface has been captured with the help of LCT system. Specimens carrying similar order of roughness parameters have been used for different configurations of contacts, namely flat-flat, cylinder-flat, and cylinder-cylinder. Here again, each specimen contains single hole of 0.8 mm diameter, which were drilled radially from that backside to a depth of 24.5 mm for fixing the thermocouple, which is used for *in-situ* calibration of the liquid crystal colors. The distance between thermocouples tip and the LC sheet pasted on the test surface is estimated to be about 0.5 mm. Additional arrangements of lighting system and digital camera have been incorporated for implementing the LCT technique. One pair of halogen lights have been used as a white light source for properly illuminating the images. The background intensity in the range of 80 and 120 points on an eight bit scale (0–255) is reported to be sufficient enough to capture the true sense of colors [37], and the similar criteria have been adopted in this investigation. A high resolution digital color CCD camera with a shutter speed of 1/30 second has been used for image capturing. Encapsulated LC polyester sheet procured from LCR Hallcrest™ is used in this study. The schematic of the experimental setup, which is used for mapping the surface temperature of the test specimens by using liquid crystal thermography technique has been shown in Fig. 3.

2.3.1. Calibration of LC sheet

The color temperature response of liquid crystal should be known prior to its use for temperature measurement. Hence calibration is carried out to develop the intrinsic color-temperature response of LCs. Several investigators have been performed tests to deal with the different aspect related with the calibration of LCs, and majority of them have recommended the single point *in-situ* mode of calibration [31,33,34,40]. Here again the single point *in-situ* calibration has been performed, and a color (hue) versus temperature curve has been generated, which was applied over the entire test surface under consideration towards mapping the temperature pattern. During calibration, the LC sheet is pasted on the flat surface of a specimen, and suitably preheated with the help of heating block. Heater is switched off, once the surface temperature reaches just above the clearing point of the LC sheet. Subsequently, the specimen is allowed to be cooled, and changing temperature images of the LC sheet is recorded along with the thermocouple data acquired at the same instances, till it crosses the clearing point of the LC sheet. Eventually, the series of images are digitized with the help of in-built subroutines of MATLAB [41], and the hue information has been extracted. A region of interest (ROI) consisting of 20 × 20 pixels encircling the center of thermocouple region is selected from each images of LC sheet, and subsequently the mean value of hue (H) of the selected ROI has been used to construct the calibration graph with the help of corresponding thermocouple measurements. A typical calibration curve indicating the

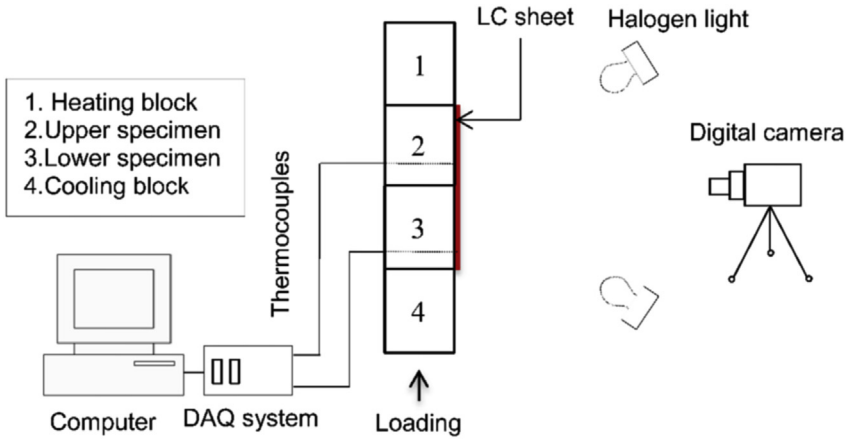

Fig. 3. Schematic of specimens with LC sheet pasted across the interface.

simultaneous variation normalized hue versus thermocouple temperature has been shown in Fig. 4. A third order polynomial curve with correlation coefficient of 0.9999 is fitted and used later to correlate surface temperature (T) and hue (H).

2.3.2. LCT experimental procedure

Experiments are performed under a typical loading condition of 0.27 kN. Single LC sheet of appropriate shape and size, covering the entire frontal surface of both of the specimens has been pasted together. To avoid any possible wrinkles in LC sheet at the interface, LC sheets have been pasted only after the application of load in each of the configurations. Thermocouples are inserted in each of the hole in upper and lower specimen from the backside, and subsequently used for LC calibration, as well as to monitor the temperature of the specimens. The 1-D heat conduction across the interface has been initiated by keeping the heater and chiller 'on' for long hours. Temperature of the heater and chiller have been preset in such a manner, that the steady state temperature of the specimen does not crosses beyond clearing points of the LC sheets in use. Sequential LC sheet images of the front surface of both the contacting bodies have been captured regularly, until the test specimens attains the steady state condition. Here again, steady state condition has been typically characterized when both the thermocouples reading does not change by 0.1 °C in 10 min. The present camera combination is able to provide very high spatial resolution temperature images, where 1 mm^2 of surface area typically represents 42 × 42 pixels; which in-turn can successfully resolve the temperature patterns with a spatial resolution of ~ 24 μm per pixel.

2.4. Data reduction

According to Mantelli and Yovanovich [42] there are three modes of heat transfer occurring at the interface of contacting solids: conduction through solid spots, convection and radiation. Therefore, the TCC, h can be expressed as below, where h_c, and h_g are the solid spot and gap conductance, respectively; and h_r is the conductance due to radiation:

$$h = h_c + h_r + h_g \quad (2)$$

The last two modes have been neglected in the study performed in vacuum environment. Therefore h_c is the thermal contact conductance due to contacting points or contacting solid spots. Whereas, conductance due to solid spots as well gap conductance are taking place in ambient. One dimensional heat transfer has been considered for all types of contact, as heat transfers from upper specimen to lower specimen. Heat flux (q) has been calculated by averaging the values of heat flux obtained from the upper and lower heat flux meter, i.e. $(q_1 + q_2)/2$. Temperatures at the contact surfaces have been obtained by the linear extrapolation of temperature data of each contacting specimens, and $\Delta T \equiv \Delta T_{extrapolation}$ is the difference of the extrapolated temperatures, i.e. at the interface. Finally, the thermal contact conductance is obtained by substituting the value of average heat flux, q and extrapolated temperature drop at the interface, in equation (1). Heat loss through specimens has been obtained by calculating the maximum difference of heat flux of upper and lower heat flux meter. In case of LCT measurement where the higher spatial resolution of this optical based non-intrusive technique ensures precise temperature drop measurements, $\Delta T \equiv \Delta T_{extrapolation}$, even very close to the interface and provide better insight of the phenomenon which forms the scope of present investigation.

2.5. Experimental uncertainty

The uncertainty of an entity depends on several independent variables. The major source of uncertainty in the estimation of TCC is due to error in the temperature drop as well as due to the heat loss to the surroundings owing to convection, conduction, and radiation losses through the complete test column/specimens [38,43]. Eventually, the error in thermocouple locations, extrapolation error of the temperature drop across the interface, misalignment of the specimens, non-conforming surfaces, and uncertainty in column diameter are the additional factors to account for predicting the overall uncertainty in estimating the TCC [10,11]. The effects of the latter three factors has been tried to overcome by suitable designing/manufacturing efforts and are expected to be insignificant in the present analysis. Table 3 illustrate the comprehensive assessment in the uncertainty for major quantities along with the overall uncertainty in experimental TCC while using the thermocouple sensors, which has been calculated based on the law of error propagation model by Holman [44].

Uncertainty in temperature obtained from LC data is the function of uncertainty in temperature sensor (thermocouple), LC

Table 3
Experimental uncertainties in TCC estimation.

Measured quantity	Uncertainty (%)		
	Flat-Flat	Cylinder-Flat	Cylinder-Cylinder
Temperature measurement, °C	±0.22	±0.22	±0.22
Temperature drop, °C	±2.96	±2.50	±2.25
Heat flux, W/m^2	±5.00	±5.00	±5.00
Maximum heat loss, W/m^2	±9.92	±11.11	±12.37
TCC, W/m^2.K	±12.14	±13.03	±14.07

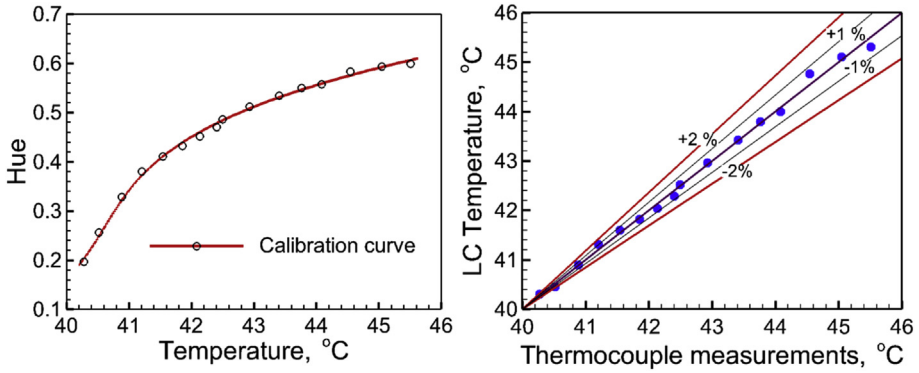

Fig. 4. Calibration curve with parity plot.

calibration and geometrical translation (correlating physical length of specimens (mm) to captured image size (pixels)). Positional inaccuracy in conjunction with the edge detection through the image pixels could be the main contributing factors towards correctly estimating temperature jump. Uncertainty in LC response is ±2 % and error in interface location is ±0.12 %. There exists inherent uncertainty in locating the correct pixel rows representing the real edge at the interface. In addition, there remains the uncertainty that the real edge may not lie exactly between two pixel rows, but in the middle of single one. This may lead to the additional rounding error in the identification of the interface, and the associated temperature jump. Assuming the measured intermediate distance between the points, which are extended to get the temperature drop and finite thicknesses of different regions is accurate to the extent between 1.0 and 5.0 pixels, the maximum uncertainty in interfacial temperature drop on the basis of LCT is estimated to be $\leq$ 4.0% (corresponding to the lowest interfacial temperature drop case). Finally, on the basis of law of error propagation [44], total uncertainty in LC temperature measurement has been calculated as ±2.02 % and thus maximum uncertainty in estimating temperature jump by LC data is around ±4.04 %.

3. Results and discussion

The experiments have been conducted in an axial heat flow apparatus as described above, and temperature measurements have been performed on the basis of thermocouples as well as LCT for three type of contact configurations, i.e. flat-flat, cylinder-flat and cylinder-cylinder contacts. Evidently, the heater block in contact with the upper specimen heats the block from the top, and the cooling block in contact with the lower specimen cool the lower block from the bottom, and thus the 1-D axial heat conduction is initiated. Firstly, results obtained from thermocouple measurements have been discussed under varying loading conditions, and subsequently detailed 2-D temperature measurement based upon the LCT has been presented for a typical loading condition of (0.27 kN). The purpose of the LCT based measurements is to establish a good understanding of the heat transfer phenomena at the interface with much accurate estimate of TCC, and explore the capability and limitations of the technique in quantifying the micro-scale heat transfer in the proximity of the interface. To the best of our knowledge, it is the first time that LCT is being used to extract detailed quantitative information of temperature in the near proximity of the flat and curvilinear contacting surfaces under consideration.

3.1. Heat transfer across different contact models: An overview

Evidently, the thermal contact conductance depends upon, the ratio of actual contact area to nominal contact area and that depends upon several geometric, thermal and mechanical parameters such as; geometry of the contacting solids (surface roughness, asperity slope and flatness deviation), contacting pressure, gap thickness, thermal conductivities of the contacting solids and interstitial fluid, type of interstitial fluid or material (vacuum, grease, foils, etc.), hardness or yield strength of the contacting solids (which affects the plastic deformation of the asperities), modulus of elasticity of the contacting solids (which affects the elastic deformation of the asperities), average temperature of the interface, linear coefficient of thermal expansion [20]. Present experimental investigation provides the reliable dataset of TCC under the varying loading conditions for different contact models (Fig. 1) carrying diverse nominal contact area with similar degree of roughness parameters, while assuming the one dimensional steady state heat flow across the interface.

The variation in TCC for flat-flat versus two types of line contact models, i.e. cylinder-flat and cylinder-cylinder under the application of normal load ranging in between 0.274 kN and 3.924 kN has been shown in Fig. 5. Overall, it has been observed that TCC is increased with pressure for all of the test configurations, however the percentage improvements are found to be highest ($\sim$ 900%) for the flat-flat contact model. The lowest improvement ($\sim$ 112%) is restricted for cylinder-cylinder contact which is supposed to provide a clear line contact (reduced area of contact) due to curvilinear geometry for both of the specimens. The value of TCC at minimal load of 0.274 kN are 2.588, 1.813 and 1.682 kW/m^{2}K for flat-flat, cylinder-flat and cylinder-cylinder contacts respectively. Additionally, the values obtained for flat surfaces in contact are higher by almost an order of magnitude against the curvilinear contact at the maximum load. Similar observation were reported earlier [14], and the reason to this is attributed to the fact that; when curved surfaces are in contact, the heat flow constrained to flow across the line contact region, which limits probability of asperities contact. Recent scale-resolved direct numerical simulation (DNS) of thermal transport across the interface [21] confirms that the TCC is strongly governed by the number of contacts, and only weakly by the size or shape of the contacting asperities. In the present investigation, all of the three shapes of specimens have been created by the same manufacturing process i.e. wire electrical discharge machining (EDM), hence an uniform distribution of number of asperities per unit nominal contact area is quite likely. Evidently, higher thermal contact conductance of flat-flat surface contact represents contact zones with more uniformly distributed denser contacts as against the corresponding cylinder-flat and cylinder-cylinder contacts. Therefore, the nominal contact area will be the major parameter for change in the TCC between different contact models.

Here, the nominal contact area for flat-flat contact is expected to be relatively large, hence more asperities would be coming together into contact leading to higher real area of contacts, and consequently higher values of TCC when compared with rest of the two configurations. The investigation of Gee et al. [15] had proposed the line-contact model for the cylinder-flat contact, and concluded that at lighter load the line-contact between the cylinder-flat contact results in terms of small elliptical contact area (crowning), which grows and changes shape until it becomes essentially the long narrow rectangular contact assumed in the theoretical analysis. The higher resistances measured at light loads were attributed to errors of form (crowning) along the longitudinal

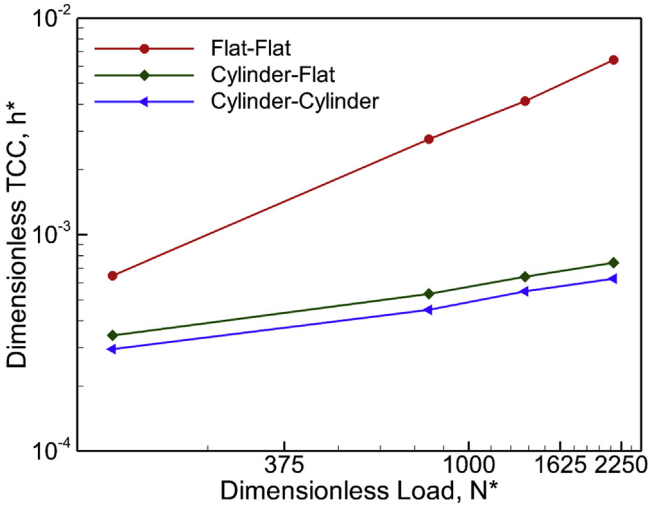

Fig. 5. Effect of loading on thermal contact conductance.

contact line of the semi-cylinder that were supposed to provide a much greater constriction to heat flow. Similarly on the basis of the Hertz theory of contact [45], it is quite likely that the a theoretical line contact will exist between the cylinder-cylinder contacts when the models are subjected to the lighter loading condition, and hence *lesser* number of asperities would come under the influence of direct contact along the interface, that will lead to the significant difference in TCC as compared to the cylinder-flat contact.

However at higher loading conditions, crowning effect will get diminished and the typical line contact for both of the curvilinear contact will deliver long narrow contact strip of similar dimensional scale; and hence alike number of asperities would come under contact, and offer alike real contact area under the influence of elastic/plastic deformation of individual asperities. Therefore, the degree of disagreement in TCC between the cylinder-flat versus cylinder-cylinder get diminished (Fig. 5) at higher loading conditions.

3.2. Heat transfer at the interface: A close-up-view

This part of the paper deals with the close-up view of the 1-D/2-D temperature distribution at the cusp of interface in the best possible manner with the help of qualitative and quantitative LCT measurements. Color images of the specimen pasted with LC sheet has been captured at regular time intervals during the heat transfer experiments till it attains the steady state conditions; and few of the selected images illustrating the respective change in temperatures of each configurations are shown here in Fig. 6. It is important to note that each of the configurations take independent span of time to start displaying the color which can be used to get the quantitative representation of temperature, until it attain the steady state condition. In the colored images, blue indicates the hottest regions, followed by yellow, green, red, and black respectively for decrease in the temperatures. Evidently, the effect of heating/cooling of specimens are represented by the transient color images, where the sequential color shows the change in temperature for the respective block until the attainment of steady state condition. The transition of colors in the upper specimens of each set from green to blue represents the influence of heater, and black/red to green in the lower specimens represent the influence of recirculating chilled water. These heater and chiller devices work in tandem to establish the heat flow across the interface.

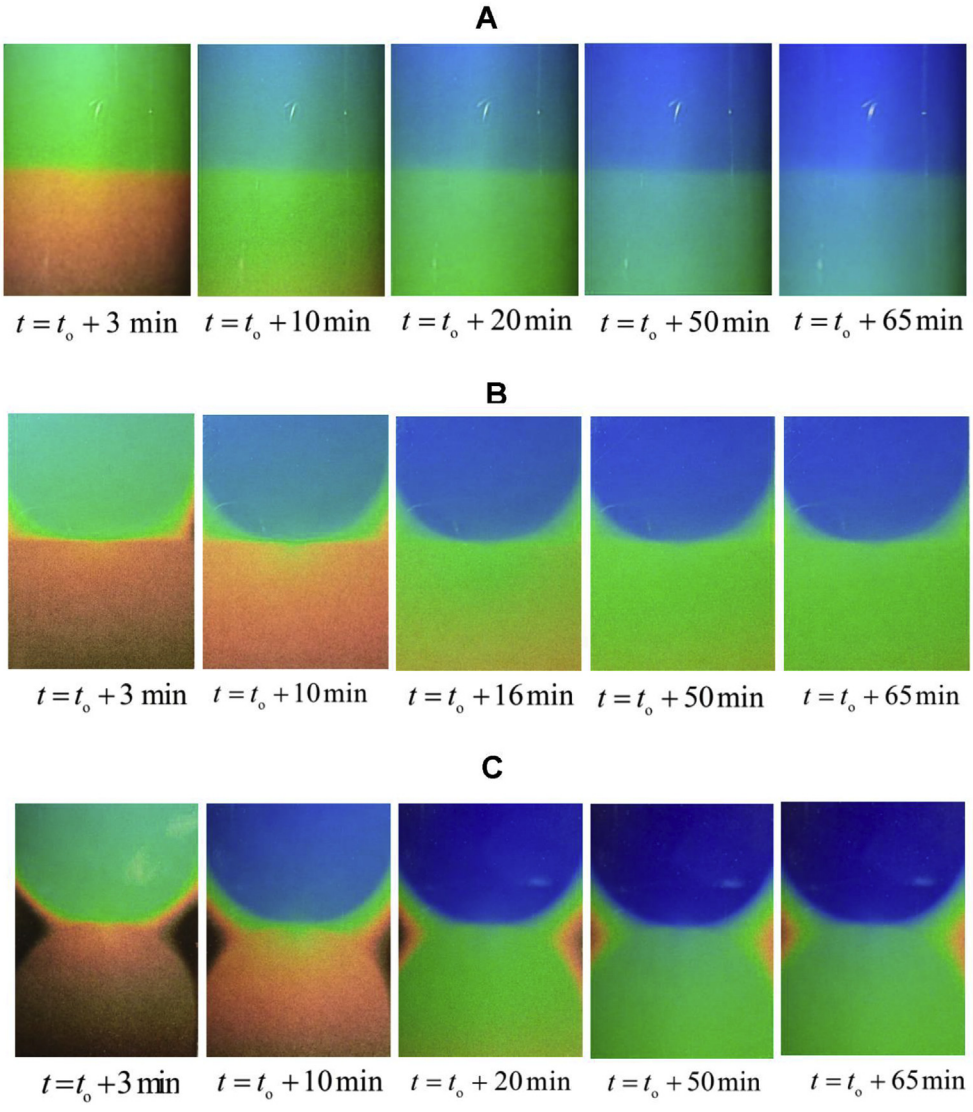

Fig. 6. LC images of A. Flat-Flat, B. Cylinder-Flat, and C. Cylinder-Cylinder contacts at different time steps.

Contact at the interface for each configurations is clearly visible in these temperature images, where sharp color change at the junction of upper and lower specimen indicates the temperature jump across the contact. Evidently, the temperature difference acts as the driving potential for heat transfer, and heat flows as the current imposed by that potential. Therefore, these temperature images of the conduction heat transfer provide an important information, and might help in performing the analysis on the basis of possible isotherms; as the heat flux lines can be easily obtained or visualized as being perpendicular to these isotherms. In this regard, the temperature changes all across the intermediate space between the curvilinear edge shows the typical heat transfer from the upper hot surface of the cylinder to the lower cool surface of the flat/cylinder specimen through the empty space. While, lateral conduction through the LC sheet is supposed to be negligible (as discussed earlier in sec 2.3), and thus it provides clue for the intermediate heat flux lines. If we assume the entire cylinder-flat and cylinder-cylinder joint region as a series of parallel flux-tubes, then entire flux tubes can be divided into three different zones (i.e. upper cylindrical body surface, interstitial fluid and lower flat/cylinder body). Henceforth, an argument can be made that the intermediate zone filled with atmospheric air also participate and allows the heat flow from the upper block to the lower one which might be through the convection/radiation mode of heat transfer. In addition, these LC images also depicts the interesting heat flow lines even at the spot of curvilinear line contacts, which are more profound for cylinder-cylinder contact.

Fig. 7 represents the variation of span-wised averaged centerline hue value with respect to the axial distances in the direction of heat flow at different time intervals, where interfaces are typically represented by the '0' (zero) value on the *x*-axis. Each centerline hue value typically represents the mean value of 40 pixels in the span-wise direction, *x*, and thus eliminate the effect of any possible intermediate noise in the pixel values, if it occurs. The smooth and continuous variation of data point indicate the quality of the measurement. The profiles from bottom to the upward direction, which is in the typical sequence from the onset of initiating heat flow/display of color to the last steady state profile, and represents the *evolution of temperature* until it attains the steady state condition. The last sequence of profile superimposed one onto another in each of the configurations, confirms the attainment of steady state conditions. The wider gap between the early to the later (steady state) temperature profile in the lower specimens as compared with the upper specimens can be regarded as the indication of the lesser rate of heat inflow due to restricted contact area. The in between curves clearly illustrate the transient nature of heat flow (temperature distribution) within blocks. Evidently, the indication of deep valley shaped profile in the lower specimen typically characterize the onset of initiating heat flow/display of color, which diminishes quite early in the flat-flat configuration as compared to the curvilinear contacts. It can be concluded that the retarded rate of heat penetration in the lower specimen during curvilinear contact configurations offer strong resistances in the heat flow due to restricted contact, and therefore it takes longer duration to attain the flatter profile as compared to the flat-flat configuration. Based upon these profiles, it can be inferred that the most profound temperature jump might exist for cylinder-cylinder configuration, followed by the cylinder-flat configuration. Evidently, each of the configurations take independent span of time to attain the steady state condition, which can be attributed to the difference in nature of contacts leading to the change in TCC estimates in all the three combinations. Once the steady state condition is confirmed, magnitude of the interfacial jump gets stabilized; which forms the basis of evaluating the temperature gradient precisely at the interface in the best possible manner.

Eventually, once the temperature (color) distribution get stabilized, the final steady state images has been converted into the corresponding hue patterns (Fig. 8), where the shapes of the

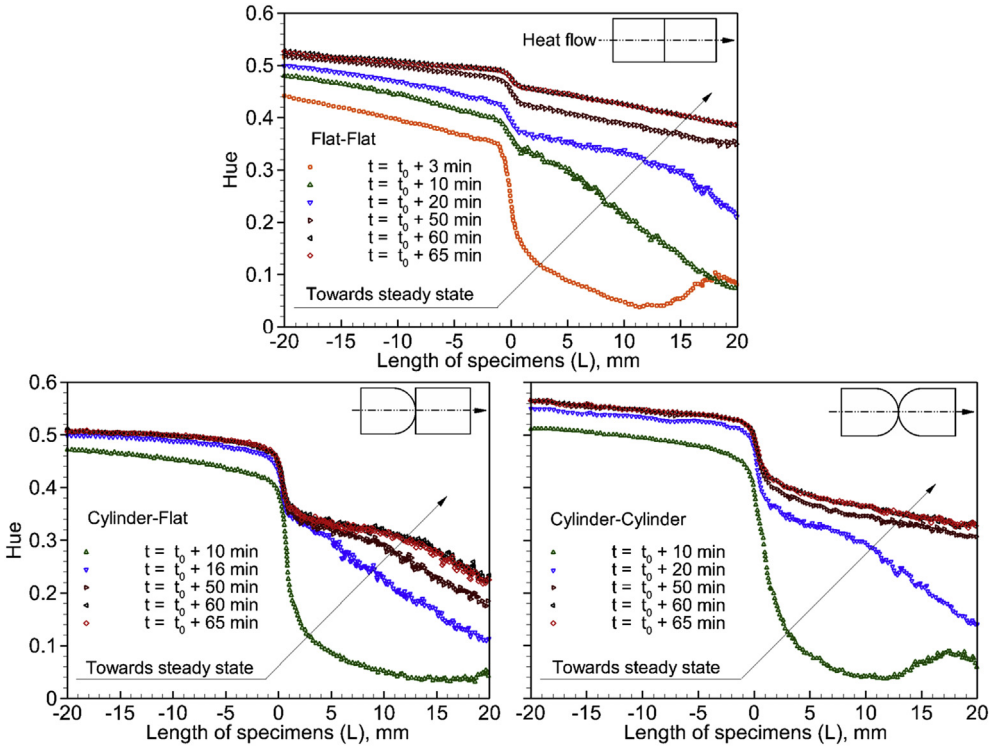

Fig. 7. Centerline hue plot at different time interval for different contacts.

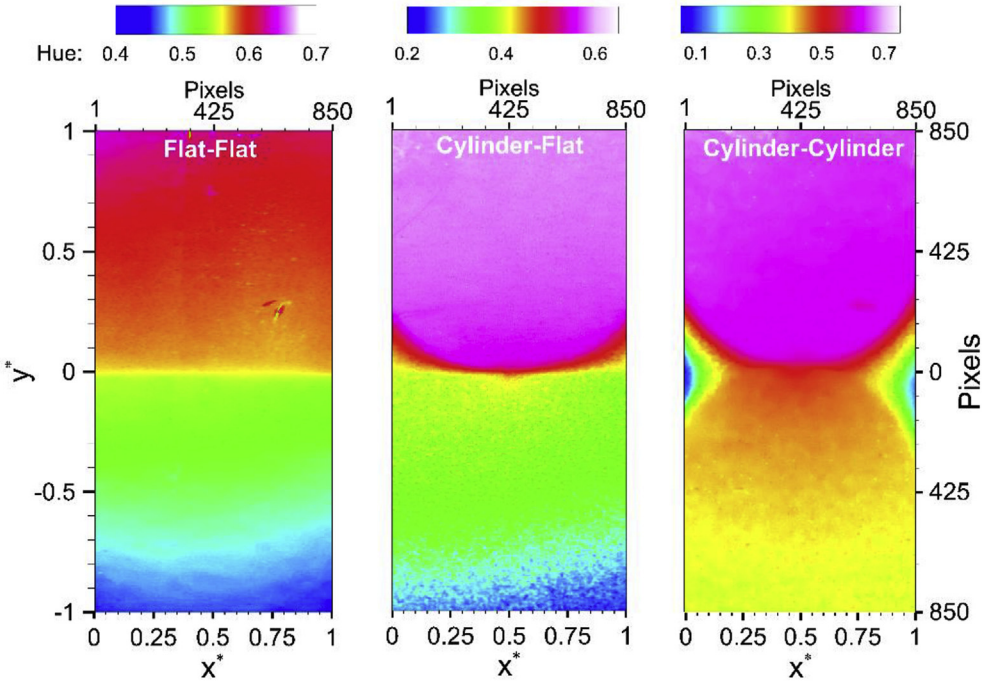

Fig. 8. Hue plots of different configurations contact under steady state.

specimens at the interfacial edge are found to be profound and distinct. Hue is related to the temperature with the help of calibration curve, and therefore the representation of color in terms of hue contours can be treated as an in-direct representation of the 2-D temperature patterns of the specimen across the interface. In this way, Fig. 8 represents the temperature distribution across the interface in the axial as well as in the lateral directions, where x^*, and y^* is the suitable non-dimensional length with respect to the respective axial and lateral dimensions of the specimen. The curvilinear contacts offer higher resistance against the heat flow in comparison to the flat-flat contacts, which can be observed in terms of profound color line at the edges of the specimens. As against the raw LC images, here the temperature gradient on the surfaces of the specimens are more distinct in the axial as well as in the lateral directions with sharp temperature jump at the edges. It is important to highlight that although due care has been taken to identify the interface through the 2-D hue distribution, but there remains inherent uncertainty that the real edge may not lie exactly between two pixel rows, but in the middle of single one.

3.3. Heat transfer at the interface: A quantitative perspective

Subsequently, the steady state 2-D surface plot of hue (Fig. 8) has been converted into the 2-D temperature contours; and the temperature data of a typical centerline longitudinal strip (1700×40 pixels) carrying an approximate width equivalent to 'a millimeter' across the specimens have been plotted in Fig. 9. As discussed earlier, it is quite likely that a line contact having finite width will exist between the existing curvilinear contacts. In the pretext of present loading and specimen conditions, it can easily be inferred on the basis of Hertz theory of contact [15,45], that the total contact width would be only of the order of hundred microns. Therefore, present width of the temperature contours (Fig. 9) suitably represent the maximum possible contact area at the centerline, which allows the axial heat flow sufficiently from upper to the lower specimen along the interface during curvilinear contacts. The finer change of temperature distribution in the longitudinal directions are clearly depicted in these surface contours, and looks very promising where every pixel of images represents temperature which is physically impossible with any intrusive way of measurements. Fieberg and Kneer [19] had reported the presence of high level noise in the IR based *transient* temperature measurement in the vicinity of the interface, that lead to the loss of information in terms 50-100 μm adjacent to the contacts. In comparison to the *transient* IR based analysis, present *steady state* LC measurement appears to contain quite stable data even at the interface. Henceforth, present *steady state* LC data appears to contain relatively very low noise level at the interface, hence the order of uncertainty in predicting the temperature drop precisely around the interface is expected to be quite low.

Furthermore, the laterally averaged value of temperature has been plotted along the axial distances and shown in Fig. 10. The upper and the lower segment of the axial temperature profile starting right from the top and the bottom end of the graph has been suitably fitted with a linear curve. It has been observed that heat flows uniformly from top to the bottom of the each specimens with a linear variation altogether, indicating the suitability of classical Fourier conduction law within the bulk region of the specimen. Subsequently, when the line is extended up to the interface, it provides an accurate estimate of $\Delta T_{\text{extrapolated}}$, otherwise helps in distinguishing the separation region where dramatic variation in temperature distribution occurs. Here the periphery of the separation region is typically designated by $x_H|_{\text{upper}}$ and $x_C|_{\text{lower}}$ on the axial co-ordinates, and the intermediate region with the data points have been shown together on the enlarged scale within Fig. 10. Evidently, the temperature distribution within the separation region is considerably different for each case. Further, it refutes the possibility of diffusion-type sharp interfacial temperature jump condition between the mating ends. The experimental results of rapidly varying but continuous profile of temperature seems very promising for the future development of the model, and restricts the possibility of using the extrapolated temperature profile with

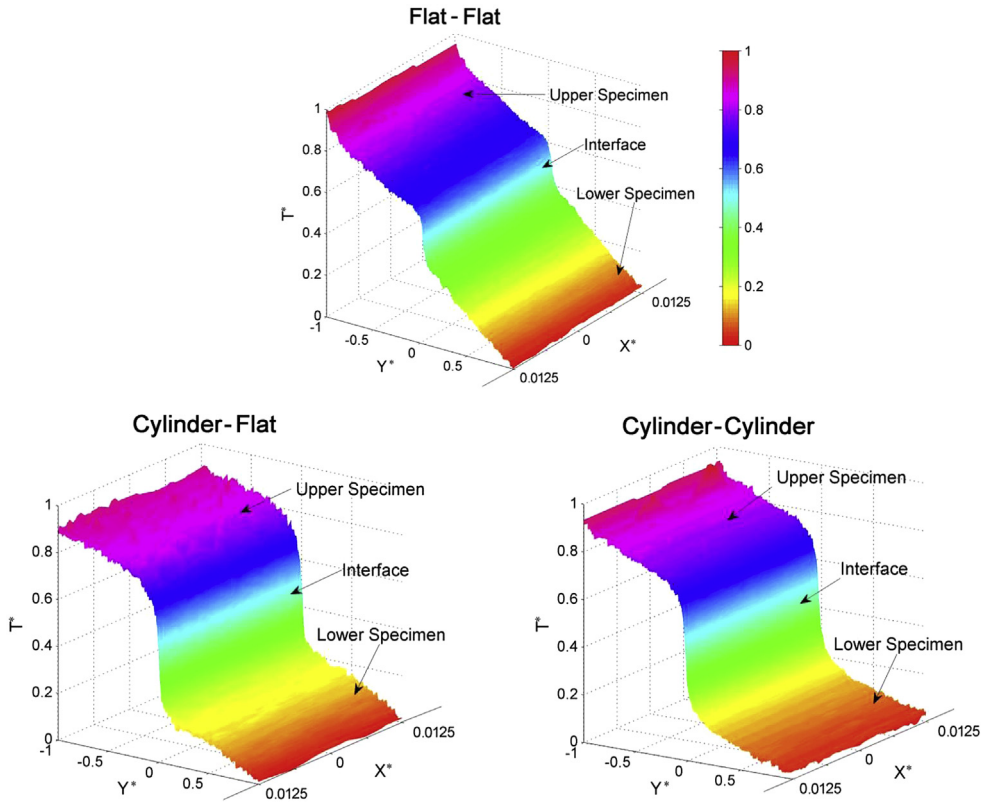

Fig. 9. Steady state surface temperature contours of different configurations in contact.

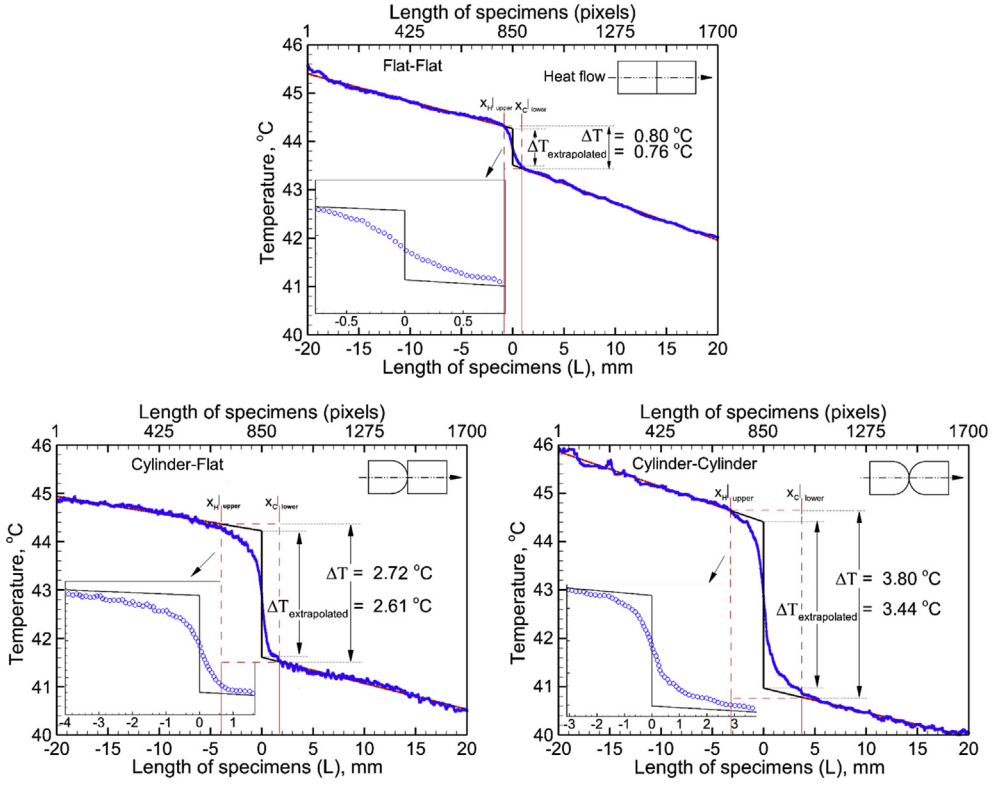

Fig. 10. Steady state axial temperature plot for different configurations across interface.

Fourier heat conduction models to get the solutions in the near vicinity of the contacting boundaries. The temperature profile for the flat-flat and cylinder-cylinder combination appears to be approximately axisymmetric around the interface line, whereas

cylinder-flat shows asymmetric nature of curve with remarkably different degree of slope in each of blocks. These observations are quite understandable, and can be explained on the basis of geometrical symmetry/asymmetry of the specimen with respect to the contact -plane/-line at the interface. Evidently, the slope of the temperature profile can be regarded as the indication of axial heat flow along the specimen. In this connection, it is important to highlight that the change in the degree of slope of upper specimen with that of the lower specimen is not always in tune with the general perception of decreasing rate of heat flux between each block in the direction of heat flow. Similar findings were reported earlier in a typical TCC experiments performed at moderate interfacial temperature, i.e. interfacial temperature ~ surrounding temperature [46] with low temperature drop situation at the interface. The prevailing thermal condition resulted in terms of higher heat flux reading through the lower specimen, as against the heat inflow through the upper specimen. Fig. 10 shows the similar discrepancies in the heat flux balance sheet for the flat-flat, and cylinder-flat contact configurations, where the interfacial temperature jump are relatively less and mean interfacial temperature is moderate. It appears that under the influence of given boundary and initial conditions, the 1-D axial heat flow assumption retract towards multidimensional heat conduction with additional gain from the environment. Based upon these LCs measurements (Fig. 10), a gradual nonlinear transition in the temperature variation has been noticed within the separation region up to the proximity of the interface, where again slope of the curve changes significantly.

3.4. Effective thermal conductivity: An alternative estimate of TCC

To deal with the nonlinearity in the separation region, the concept of effective thermal conductivity, k_{contact} across the interface has been derived from thermal resistance based formulation [21], i.e.

$$k_{\text{contact}} = \frac{\delta_{\text{contact}}}{\left(\frac{\Delta T}{Q/A} - \frac{\delta_{\text{H}}|_{\text{upper}}}{k_{\text{H}}|_{\text{upper}}} - \frac{\delta_{\text{C}}|_{\text{lower}}}{k_{\text{C}}|_{\text{lower}}}\right)} \tag{3}$$

where A is the apparent area of contact; $\delta_{\text{H}}|_{\text{upper}}$ and $\delta_{\text{C}}|_{\text{lower}}$ is the height of the microscale model of the top and bottom zones at the interface containing asperities with thermal conductivity values as $k_{\text{H}}|_{\text{upper}}$ and $k_{\text{C}}|_{\text{lower}}$, respectively; δ_{contact} is the overall span of the interface (effective material gap); and ΔT is temperature difference between the separation region during which temperature gradient depart from its linearity established in the bulk of two surfaces. Inherently, the ratio $k_{\text{contact}}/\delta_{\text{contact}}$ is nothing but the TCC at the interface which formed the basis for estimating the effective thermal conductivity across interfaces, k_{contact} (i.e. thermal conductivity of the effective material in the gap). Evidently, in most of the commercial CFD/CHT codes, contact resistance is modeled as the resistance offered by an effective material gap of finite thickness (δ_{contact}) between the two surfaces in contact, in which case, the thermal conductivity of the effective material in the gap (k_{contact}) must be specified by the user. However, for all practical purposes conventional thermocouple technique fails to resolve the δ_{contact} experimentally, and also carries greater extrapolation error in estimating the temperature gradient, $\Delta T_{\text{extrapolation}}$ at the interface (which might be $\sim$ 20% [10,17]). And, therefore due to its finer spatial resolution and significant lower measurement errors, present LCT based investigation can be seen as potentially powerful non-invasive solution to experimentally resolve the interface in terms of δ_{contact}, ΔT and $\Delta T_{\text{extrapolation}}$, and might be treated as a baseline database. Certainly, the present measurement of $\Delta T_{\text{extrapolated}}$ on the basis LCT data can be taken as the better representation of temperature jump as compared to extrapolation performed on the basis thermocouple data.

Eventually, in order to capture the finer details in the near proximity of the interface and within separation region, the temperature contours have been plotted again on an expanded scale, and shown in Fig. 11. The nonlinear temperature transition can be observed in much better manner through these surface plots (Fig. 11), where the different regions are found to be visually profound and distinct. Furthermore, based upon the enlarged views within Fig. 10 and corresponding surface plots, the finite thicknesses of different region, i.e. $\delta_{\text{H}}|_{\text{upper}}$, $\delta_{\text{C}}|_{\text{lower}}$, and δ_{contact} have been identified in terms of pixel resolution, which is subsequently converted into the length scale (μm) on the basis of the size of each pixels. It is important to highlight that in cited investigation [21], the mean roughness height was chosen as the arbitrary value for δ_{contact} during the extraction of k_{contact}. Inherently, the actual numerical value of k_{contact} and δ_{contact} were found to be apparently irreverent, because the ratio of duo represents the TCC which matters the most. Therefore, once the value of TCC was attained on the basis of scale resolved simulation, the value of k_{contact} had been evaluated while taking the TCC and δ_{contact} into account.

Present LC measurement shows the presence of distinct isotherm region at the interface, which act as a buffer zone in between the region of abrupt temperature change. The finite widths of these isotherms are found to be sufficiently large in size as against the individual pixel size of the image, and the region comprises of significant numbers of image pixels (~30±1) in the axial direction, which effectively represent an overall length equivalent to ~700 – 900 (±5) μm for each of the configurations. This shows the effect on the heat flow for each contacting boundaries much beyond the asperities mean height in the adjacent proximity of the interface. Henceforth, in the present work characteristic length for δ_{contact} has been typically selected on the basis of the size of clearly defined distinct temperature region around the interfaces. Consequently, equation (3) has been used to compute the effective thermal conductivity, and thus the mean value of TCC has been obtained as the ratio of k_{contact} and the δ_{contact}. Eventually, an independent estimate of TCC while using LC data has been obtained again on the basis of substituting extrapolated temperature drop measurement $\Delta T_{\text{extrapolation}}$ in equation (1), and results are presented along with the assessment of aforementioned parameters in Table 4. Here, the values of heat fluxes (q_1, q_2) has been suitably obtained on the basis of LC based axial temperature measurements, while using the classical Fourier's law of heat conduction, i.e. $-k\frac{dT}{dx}$. As discussed in section 2.5, there exists an uncertainty in assigning the correct pixel-row with that to the real edge, which finally contributes for an additional uncertainty in fixing the finite thicknesses of different regions, i.e. $\delta_{\text{H}}|_{\text{upper}}$, $\delta_{\text{C}}|_{\text{lower}}$, and δ_{contact}, and henceforth should be taken into account during the uncertainty assessment of TCC. In this regard, different value of $\text{TCC}|_{k_{\text{contact}}/\delta_{\text{contact}}}$ has been evaluated by arbitrary changing the characteristic length of δ_{contact} in terms of ± 2 pixel-rows within the periphery of the separation region (along with respective estimate of k_{contact}). At the end, the results are compared in Fig. 12 to ascertain about the robustness of the present methodology while accounting the uncertainty associated with selection criteria of δ_{contact}.

Overall, it has been observed that the effect of the contact nature have definite impact on these parameters. The periphery of the separation region, is quite restrictive in the flat-flat contact model as compared to the curvilinear contact models, and effective thermal conductivity is found be highest with consequential effect on the TCC. The distance of separation region's periphery (point $x_{\text{H}}|_{\text{upper}}$ and $x_{\text{C}}|_{\text{lower}}$) from the interface are never precisely same,

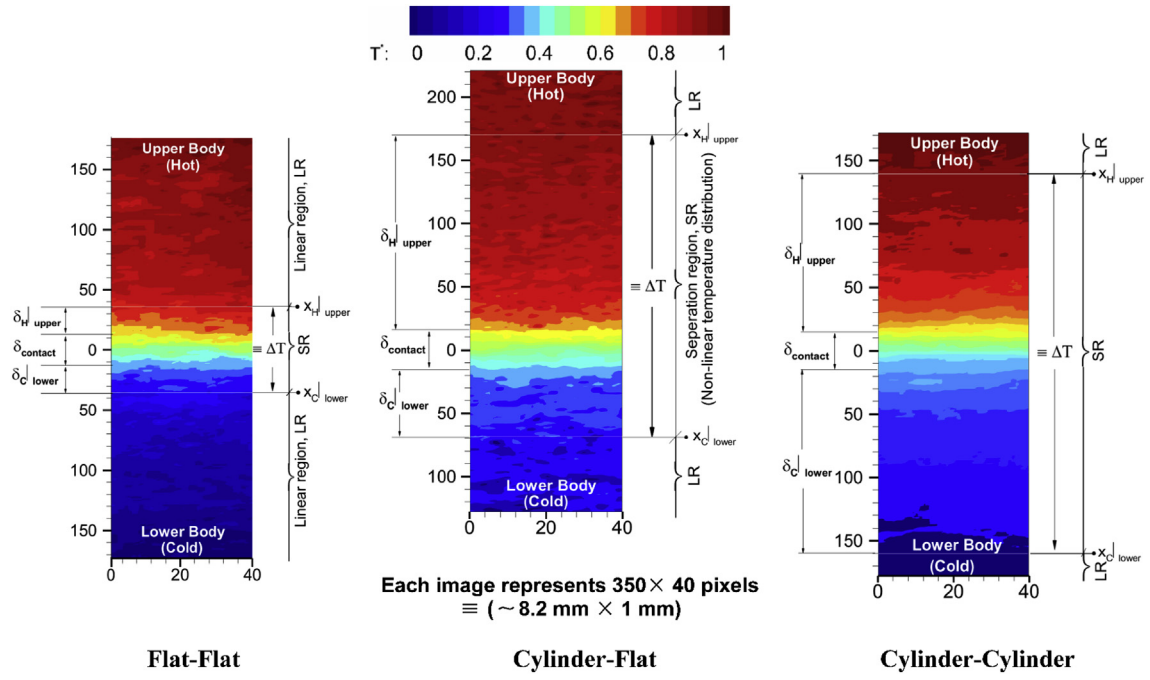

Fig. 11. Temperature contours showing interface regions on an expanded scale.

Table 4
TCC analysis parameters of different contact configurations.

Configurations	$\lvert\delta_H\rvert_{upper}$ (μm)	$\lvert\delta_C\rvert_{lower}$ (μm)	$\delta_{contact}$ (μm)	$k_{contact}$ (W/mK)	$\frac{k_{contact}}{\delta_{contact}} \equiv TCC\lvert_{\frac{k_{contact}}{\delta_{contact}}}$ (W/m^{2}K)	$TCC\lvert_{\Delta T_{extrapolation}}$ (W/m^{2}K)
Flat-Flat	777	871	713	6.537	9168.1	8828.2
Cylinder-Flat	3974	1648	695	1.474	2120.7	2031.2
Cylinder-Cylinder	3272	3813	869	1.624	1869.0	1854.6

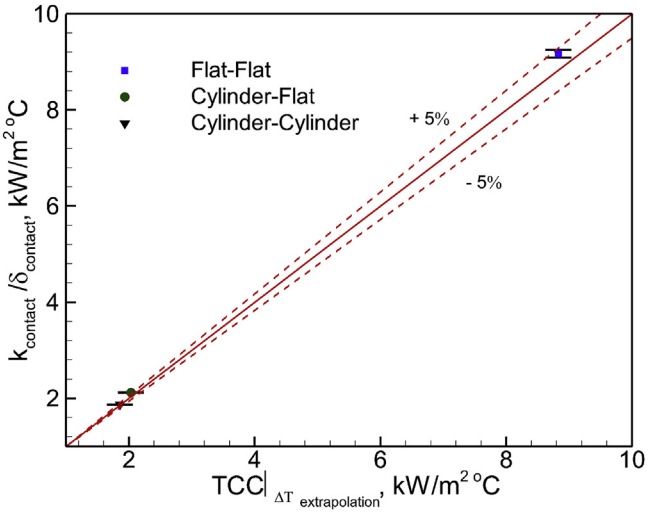

Fig. 12. Parity plot between TCC by extrapolation and TCC by effective thermal conductivity.

even the profile of the specimens are axisymmetric about the interfacial plane/line, the reason can be associated with the difference in the rate of 'heat-supply' versus the 'heat-extraction' at the non-contacting ends of the specimen. However during cylinder-flat contact model (which is the geometrically asymmetric about the interface), a remarkable difference in the distance of $x_H|_{upper}$ and $x_C|_{lower}$ with that of the interfacial line has been observed. This indicate that even the geometrical symmetry of the contact model around the interface have the significant influence on the temperature distribution around the contact spot. It is interesting to observe that the effective conductivity does not follow the similar trend as that of the TCC, which need further examination through additional set of experiment by varying the different parameters. The detailed investigation with wider set of varying parameters namely, roughness, curvature, contact pressure, and interfacial temperatures are underway, and it is expected to provide better understanding of the mechanism and estimate about TCC on the basis of liquid crystal thermography.

Certainly, there exist various difficulties in the implementation of LCT for the TCC investigation, and it also carries many of limitations associated with the technique. However, in view of the vast amount of its exciting information, it surpasses the all. Following is the list of omissions, assumptions and approximations, which has been taken into account towards exploring the field of TCC based upon LCT measurements:

1) Rounding error in detecting specimen's edges has not been considered.
2) Conduction in LC sheet and its effect on heat transfer, especially in the curvilinear geometry has been assumed to be negligible.

3) A possible convection loss at the surface of the specimen has not been taken into consideration, and neglected in the analysis.
4) Due to the limiting bandwidth criteria of LC sheets, the experiment has been performed at low temperature, hence restrict it the usage for high temperature experiments.
5) The heat transfer through the specimens is assumed to be axially one-dimensional.
6) Temperature jump has been calculated by using surface pasted LC sheets, whereas in conventional approach the interfacial temperature jump is routinely evaluated on the basis centrally placed thermocouples at different axial locations. During measurements, a temperature difference between the axially inserted centerline thermocouples and its corresponding temperature at the surface of LC sheet shows a maximum difference of about 0.15°C, which is about 0.4% of the centerline temperature with negligible discrepancy in the temperature jump measurement at the interface. Similar findings were reported earlier during TCC estimation on the basis of IR based surface measurements [26].
7) Due care has been taken to identify the interface through the 2-D temperature distribution, but there remains the uncertainty that the real edge may not lie exactly between two pixel rows, but in the middle of single one. This may lead to the rounding error in the identification of the interface on the basis of hue/temperature matrix.

4. Conclusion

Experimental investigation of TCC between two brass specimens with three different pairs of contact models, namely flat-flat cylinder-flat, and cylinder-cylinder contacts have been performed. The study make use of steady state approach for TCC estimation on the basis of extrapolated temperature measurement at the interface. Firstly, the experiments have been performed under varying loading conditions on a well standardized setup with thermocouples and a reliable dataset for TCC between curvilinear contacts has been generated, which is also compared against the conventional flat-flat contact results. Overall, it has been observed that TCC is increased with loading for all of the test configurations, however the percentage improvements are found to be highest for the flat-flat contact model. The values obtained for flat surfaces in contact are found to be higher by almost an order of magnitude in reference to the cylinder-cylinder contact at the maximum level of loading condition. The higher resistances measured at light loads were attributed to errors of form (crowning) along the longitudinal contact line of the curvilinear contacts, which constrained the heat flow along the contact spot. The difference in TCC between both the curvilinear contacts is found to be larger at lighter load, which diminishes well at the higher loading values.

In the latter half of the study, a close-up perspective of the heat transfer between the different contacts under investigation have been explored on the basis of LCT. Interesting heat flow lines passing through the contact configurations are captured with the help of transient LC images. The 'non-linear' steady state axial temperature profile around the interface has been captured with greater precision, and consequently the bandwidth of distinct temperature region representing the effective material gap at the interface is identified. Due to its finer spatial resolution and significant lower measurement errors, present LCT based investigation can be seen as potentially powerful non-invasive solution to experimentally resolve the interface in terms of $\delta_{contact}$, ΔT and $\Delta T_{extrapolation}$, and might be treated as a baseline database for validation with the upcoming scale-resolved numerical heat transfer solutions. Additionally, the significant effect of change in nominal cross sectional area during cylinder-flat and cylinder-cylinder contacts on the nature of dT/dx slope around the interface, fortify the need for accounting the effect of change in area during analysis for future researchers, to get the better TCC estimate.

Present steady state results for different-but exemplary-contact models reveal the LCT's ability to determine the TCC with precise temperature drop measurements closer to the interface. Eventually, on the basis of thermal resistance based formulation, present LC experiment provides a reliable estimate of effective thermal conductivity of the interface, and an independent methodology of TCC estimation. The value of effective thermal conductivity would help strategically the user of the commercial CFD/CHT codes in the successful thermal modeling of the interface. The comparison between the two different methodologies of TCC estimation shows strong agreement, and thus establishes the LCT technique as promising tool to get the insight of the interfacial heat transfer. With the experimental setup and analysis methods introduced, further studies on TCC with LCT are underway, which includes the effect of roughness, curvature of the curvilinear contact profiles, contact pressure, and etc.

Acknowledgements

The authors gratefully acknowledge the financial support of the Bhabha Atomic Research Centre (BARC), India, vide project grant Code: DAE-855-MIED for initiating this research activity in Mechanical & Industrial Engineering Department (MIED) at Indian Institute of Technology (IIT) Roorkee, India. The authors also acknowledge the support of IIT Roorkee in order to improve the laboratories and help in initiating the research based upon liquid crystal thermography in MIED.

References

[1] Yovanovich MM. Four decades of research on thermal contact, gap, and joint resistance in microelectronic. IEEE Trans components Packag Technol 2005;28:182–206.
[2] Fletcher LS. Recent developments in contact conductance heal transfer. J Heat Transf 1988;110:1059–70.
[3] Cooper M, Mikic BB, Yovanovich MM. Thermal contact conductance. Int J Heat Mass Transf 1969;12:279–300.
[4] Mikic B. Thermal contact conductance; theoretical considerations. Int J Heat Mass Transf 1974;17:205–14.
[5] Jeng Y, Chen J, Cheng C. Theoretical and experimental study of a thermal contact conductance model for elastic, elastoplastic and plastic deformation of rough surfaces. Tribol Lett 2003;14:251–9.
[6] Sadowski P, Stupkiewicz S. A model of thermal contact conductance at high real contact area fractions. Wear 2010;268:77–85. http://dx.doi.org/10.1016/j.wear.2009.06.040.
[7] Sridhar MR, Yovanovich MM. Elastoplastic contact conductance model for isotropic conforming rough surfaces and comparison with experiments. J Heat Transf 1996;118:3–9.
[8] Yuncu H. Thermal contact conductance of nominally flat surfaces. Heat Mass Transf 2006;44(1):1–5.
[9] Misra P, Nagaraju J. An experimental study to show the effect of thermal stress on thermal contact conductance at sub-megapascal contact pressures. J Heat Transf 2010;132:094501.
[10] Tariq A, Asif M. Experimental investigation of thermal contact conductance for nominally flat metallic contact. Heat Mass Transf 2016;52:291–307.
[11] Asif M, Tariq A. Correlations of thermal contact conductance for nominally flat metallic contact in vacuum. Exp Heat Transf 2016;29:1–29.
[12] Ayers GH. Cylindrical thermal contact conductance. Texas: Texas A&M University; 2003. M.S. Thesis.
[13] Madhusudana CV. Thermal conductance of cylindrical joints. Int J Heat Mass Transf 1999;42:1273–87.
[14] Sunil Kumar S, Abilash PM, Ramamurthi K. Thermal contact conductance for cylindrical and spherical contacts. Heat Mass Transf 2004;40:679–88.
[15] Mcgee GR, Schankula MH, Yovanovich MM. Thermal resistance of cylinder-flat contacts: theoretical analysis and experimental verification of a line-contact model. Nucl Eng Des 1985;86:369–81.
[16] Zhang P, Xuana YM, Li Q. A high-precision instrumentation of measuring thermal contact resistance using reversible heat flux. Exp Therm Fluid Sci 2014;54:204–11.
[17] Thomas TR. Extrapolation errors in thermal contact resistance measurements.

J Heat Transf 1975;97:305–7.
[18] Woolley JW, Woodbury KA. Thermocouple data in the inverse heat conduction problem. Heat Transf Eng 2011;32:811–25.
[19] Fieberg C, Kneer R. Determination of thermal contact resistance from transient temperature measurements. Int J Heat Mass Transf 2008;51:1017–23.
[20] Madhusudana CV. Thermal contact conductance. first ed. Berlin: Springer; 1995.
[21] Verma NN, Mazumder S. Extraction of thermal contact conductance of metal–metal contacts from scale-resolved direct numerical simulation. Int J Heat Mass Transf 2016;94:164–73.
[22] Tzou DY. A unified field approach for heat conduction from macro- to microscales. J Heat Transf 1995;117:8–16.
[23] Jiji LM. Heat conduction. New York: Springer; 2009.
[24] Shi L, Wang HL. Investigation on thermal contact resistance by photothermal technique at low temperature. Heat Mass Transf 2007;43(11):1179–84.
[25] Bi D, Chen H, Tian Y. Influences of temperature and contact pressure on thermal contact resistance at interfaces at cryogenic temperatures. Cryogenics 2012;52:403–9.
[26] Burghold EM, Frekers Y, Kneer R. Determination of time-dependent thermal contact conductance through IR-thermography. Int J Therm Sci 2015;98:148–55.
[27] Camci C. Introduction to liquid crystal thermography. Von Karman institute lecture series on temperature measurements; April 1996. VKI-LS-1996-09.
[28] Ireland PT, Jones TV. Liquid crystal measurements of heat transfer and surface shear stress. Meas Sci Technol 2000;11–7:969–86.
[29] Kakade VU, Lock GD, Wilson M, Owen JM, Mayhew JE. Accurate heat transfer measurements using thermochromic liquid crystal. Part 1: calibration and characteristics of crystals. Int J Heat Fluid Flow 2009;30:939–49.
[30] Hallcrest Product Information: http://www.hallcrest.com/DesktopModules/Bring2mind/DMX/Download.aspx?EntryId=159%26Command=Core_Download%26language=en-US%26PortalId=0%26TabId=163.
[31] Abdullah N, Talib ARA, Jaafar AA, Salleh MAM, Chong WT. The basics and issues of thermochromic liquid crystal calibrations. Exp Therm Fluid Sci 2010;34:1089–121.
[32] Muwanga R, Hassan I. Local heat transfer measurements in microchannels using liquid crystal thermography. Methodol Dev Validation 2006;128:617–26.
[33] Tariq A. Heat transfer enhancement and fluid flow transport phenomena behind surface mounted solid and permeable ribs. 2004. PhD thesis, IIT Kanpur, India.
[34] Tariq A, Singh K, Panigrahi PK. Flow and heat transfer in rectangular duct with single rib and two ribs mounted on the bottom surface. J Enhanc Heat Transf 2003;10–1:171–98.
[35] Tariq A, Panigrahi PK, Muralidhar K. Flow and heat transfer in the wake of a surface-mounted rib with a slit. Exp Fluids 2004;37:701–19.
[36] Ali MS, Tariq A, Gandhi BK. Flow and heat transfer investigation behind trapezoidal rib using PIV and LCT measurements. Exp Fluids 2013;54–5:1520–45.
[37] Ali MS, Tariq A, Gandhi BK. Role of chamfering angles and flow through slit on heat transfer augmentation behind a surface mounted rib. J Heat Transf 2016;138.
[38] Madhusudana CV. Accuracy in thermal contact conductance experiments-the effect of heat losses to the surroundings. Int Commun Heat Mass Transf 2000;27:877–91.
[39] Incropera FP, DeWitt DP, Bergman TL, Lavine AS. Fundamentals of heat and mass transfer. sixth ed. John Wiley and Sons; 2006.
[40] Rao Y, Zang S. Calibrations and the measurement uncertainty of wide-band liquid crystal thermography. Meas Sci Technol 2010;21:1–8.
[41] MATLAB, Version 8.6.0.267246 (R2015b) The Math Works, Inc.
[42] Mantelli MBH, Yovanovich MM. Thermal contact resistance. In: Gilmore DG, editor. Spacecraft thermal control handbook. Fundamental technologies. second ed., vol. I. El Segundo, CA: The Aerospace Press; 2002. p. 599–638.
[43] Sunil Kumar S, Ramamurthi K. Influence of flatness and waviness of rough surfaces on surface contact conductance. J Heat Transf 2003;125:394–402.
[44] Holman JP. Experimental methods for engineers. seventh ed. New Delhi: Tata McGraw Hill; 2001. p. 51–60.
[45] Shigley JE, Mischke CR. Mechanical engineering design. fifth ed. New York: McGraw-Hill; 1989.
[46] Singhal V, Litke PJ, Black AF, Garimella SV. An experimentally validated thermo-mechanical model for the prediction of thermal contact conductance. Int J Heat Mass Transf 2005;48:5446–59.

Nomenclature

A_c: Contact area, m^2
d_v: average diagonal length (indentation), μm
F: applied load, N
h: thermal contact conductance W/m^2K
H_v: Vickers microhardness, MPa
h_c: solid spot conductance, W/m^2K
h_g: gap conductance, W/m^2K
h_r: conductance due to radiation, W/m^2K
h^*: dimensionless TCC, $h^* = \frac{h\sigma}{mk}$
k: effective thermal conductivity, $k = \frac{2k_1k_2}{(k_1+k_2)}$, W/mK
L: axial length of LC image for each specimen (=20 mm), m
m: effective mean absolute slope, $m = \sqrt{(m_1^2 + m_2^2)}$, rad
N^*: dimensionless load, $N^* = \frac{F}{H_v \times d_v^2}$
P: contact pressure, MPa
Q: heat flow through contact interface, W
q: average heat flux, W/m^2
t: time, sec
t_0: time at the start of image acquisition after color appearance, min
T^*: dimensionless temperature, $T^* = \frac{T-T_{min}}{T_{max}-T_{min}}$
ΔT: temperature jump, °C
W: lateral width of LC image for each specimen (= 20 mm), m
x^*: dimensionless length, $x^* = \frac{x}{W}$
y^*: dimensionless length, $y^* = \frac{y}{L}$

Greek symbols

σ: effective root mean square roughness, $\sigma = \sqrt{(\sigma_1^2 + \sigma_2^2)}\mu m$
δ: length in the direction of heat transfer, μm

Subscripts

1, 2: upper specimen and lower specimen
min, max: minimum, and maximum
H, C: hot and cold